Int. J. Electrochem. Sci., 14 **(2019)** 205 – 218, doi: 10.20964/2019.01.23

International Journal of
ELECTROCHEMICAL
SCIENCE
www.electrochemsci.org

Preparation and Investigation of Nickel–Antimony co-doped Tin Oxide Anodes for Electro-catalytic Oxidation of Organic Pollutions

Xia Li[1], *Cairu Shao*[1], *Jiangang Yu*[1], *Kaigui Zhu*[1,2,*]

[1] School of Physics and Nuclear Energy Engineering, Beijing University of Aeronautics and Astronautics, 37 Xueyuan Road, Haidian District, Beijing 100191, PR China
[2] Key Laboratory of Micro-nano Measurement-Manipulation and Physics, Ministry of Education Beihang University, Beijing 100191, China
[*]E-mail: kgzhu@buaa.edu.cn

Received: 5 October 2018 / *Accepted:* 8 November 2018 / *Published:* 30 November 2018

Nickel(Ni) and antimony(Sb) co-doped Ti/Ni-Sb-SnO_2 electrodes were prepared by pyrolysis coating method and then investigated by scanning electron microscopy (SEM), X-ray diffraction (XRD), X-ray photoelectron spectroscopy (XPS), linear sweep voltammetry(LSV), electrochemical impedance spectroscopy (EIS) and accelerated service life test. We discussed the changes of oxygen evolution potential and charge transfer resistant on the Ti/Ni-Sb-SnO_2 electrodes in a physical perspective. The oxygen evolution potentials improved obviously. Furthermore, the failure mechanisms of the electrodes have been studied using the EIS and SEM techniques. Our study showed that the deactivation of Ti/Ni-Sb-SnO_2 electrode was mainly due to the formation of a passive TiO_2 passive interlayer between the Ti substrate and the coating.

Keywords: Titanium-based Tin oxide electrodes, DSA electrodes, Nickel, Antimony

1. INTRODUCTION

With the increase of the discharge of industrial non-degradable wastewater, the most attention has been paid to environmentally friendly regulations and strategies to solve this problem. In recent years, electrochemical oxidation technology has attracted more and more attention owing to high energy efficiency, fast reaction rate, environmental compatibility simplicity and robustness in structure and operation[1-3]. The effectiveness and the electrochemical properties of this technology depend on the activities of electrode materials towards the targeted pollutants largely. In general, a desired electrode should meet the requirements of good conductivity, high oxygen evolution potential (OEP), low-cost,

excellent stability, and superior electrochemical activity. Dimensionally stable anodes (DSA) are also known as titanium-based metal oxide anodes, which is one of the most promising electrodes. It has been widely used in various fields such as chlor alkali industry, electrolysis metallurgy, electroplate, cathodic protection and so on[4]. Generally DSA electrodes consist of titanium substrates and oxides coating (IrO_2, RuO_2, PbO_2, BDD, SnO_2) [5-16]. But the IrO_2 and RuO_2 electrodes cannot effectively degrade pollutants in wastewater due to their low oxygen evolution potential. In addition to simple preparation process, high OEP and high activities makes SnO_2 electrodes the best choice for oxidation of organic pollutants.

As we all known that SnO_2 is a typical n-type (due to its non-stoichiometry) semiconducting material with a wide band gap (3.87–4.3eV) and shows poor conductivity. Dopant ions can greatly improve the conductivity, electro-catalytic oxidation and stability of electrodes. And Sb is the most commonly used donor impurity in SnO_2 electrodes to reduce the band gap and increase the conductivity as well as electro-catalytic activity. So the Ti/Sb-SnO_2 electrodes have become the most promising choices because of easy preparation, high O_2-overvoltage, low cost, excellent electro-catalytic performance [1,3,4,16-19]. Though the Ti/Sb-SnO_2 electrodes show high effective for the electro-catalytic oxidation of organic pollutions, the short lifetime is the main issue and limits its industrial application severely. Several studies have demonstrated that in the process of electrochemical catalytic process, the formation of inert interlayer of TiO_2 with high resistivity will cause the voltage to increase rapidly and eventually lead to the inactivation of electrode. In recent years, various methods have been attempted to solve this problem [3,19,20]. These efforts can effectively increase the stability by preventing the formation of passive layer[21]. Previous reports have verified that the Sb-X co-doped SnO_2 electrodes have better performance in the electro-catalytic process (X represent the other elements, such as Ni, Mn, Ir) [4,23-28]. Shao' group has also shown that metal doping of the anode can change the concentration of oxygen vacancies in the SnO_2 crystal lattice, and influences its stability[4]. In addition, a number of studies found that the novel Ni/Sb co-doping could enhance the accelerated lifetime of SnO_2 anode, have higher onset anodic potential and generate ozone with high efficiencies at room temperature effectively [28-33]. This would allow electrochemical oxidation to take place, besides oxygen evolution. Therefore, this type of electrode is expected to have a higher reactivity for direct anodic oxidation of contaminants. In spite of successful operation of Ti/ Ni-Sb-SnO_2 electrodes, there are less systematic information concerning the role of Ni dopant on the electrochemical characteristics of Ti/ Ni-Sb-SnO_2 electrodes.

In our study, we prepared the Ti/Ni-Sb-SnO_2 electrodes by thermal decomposition method and then we investigated the effect of Ni-Sb co-doping on the crystal structure, morphology and electrochemical properties. Finally, we studied the failure mechanisms of the electrodes in detail.

2.METHODS

2.1. Electrodes preparation

All the Ti/Ni-Sb-SnO_2 electrodes were synthesized by coating pyrolysis method. Ti plates with a

dimension of 3 cm × 3 cm were used as the base metal for all oxide-coated electrodes. The plates were firstly polished using 120-grit and 500-grit sand papers sequentially, then degreased in 40% NaOH at 90 °C for 2 h, after that etched in 10% boiling oxalic acid for 1 h followed by thorough washing with deionized water and dried. The precursor solutions were mixture of $SnCl_4 \cdot 5H_2O$, $SbCl_3$ and different contents of $NiCl_2 \cdot 6H_2O$(0, 1, 2,3.5 and 5at.% relative to Sn) were chosen to prepare the precursor for the Ni–Sb co-doped SnO_2 coating and the electrodes were named as Ni0, Ni1, Ni2, Ni3.5 and Ni5, respectively.) using alcohol(10 mL) and small amount of concentrated (37%) hydrochloric acid (2mL) as solvents. The Sb was presented in the coating solution at 6 at.% relative to Sn. Precursor solutions were dropped on the Ti substrates (3 drops). When there is no obvious solution on the surface, the electrodes were dried at 110 °C for 3 min to allow the solvents to vaporize and then baked at 550°C for 10 min for coating pyrolysis. This whole procedure was repeated 15 times. Finally, the electrodes were annealed at 550°C for 1 h.

2.2. Electrodes characterization

The morphologies of Ti/Sb-SnO_2 and Ti/Ni-Sb-SnO_2 anodes were characterized by a field emission scanning electron microscopy (FESEM, S4800, Hitachi, Japan). The microstructures were measured by the X-ray diffraction analysis (XRD, XRD-6000, Shimadzu, Japan) using a diffractometer with Cu Kα radiation (λ = 0.15406 nm) and working at 30 kV/40 mA. The diffraction patterns were collected in the range of 2θ = 20–80° at a rate of 5°/min. X-ray photoelectron spectroscope (Al Kα radiation, hν = 1486.6 eV; Thermo ESCALAB 250Xi, USA) was performed to analyze the composition and chemical state of the surface elements. The spectra were calibrated with respect to the signal of contamination carbon (284.8 eV) as internal reference. The XPS core level spectra were fitted and analyzed using a XPS Peak Processing program with a Lorentzian-Gaussian peak shape after a background subtraction.

Electrochemical experiments were performed in a conventional three-electrode cell recorded by an electrochemical workstation (CHI-600E). Our prepared electrodes were employed as the working electrodes and the active areas of anodes were 1.0 × 1.0 cm^2 and the rest coating film was removed by polishing. A platinum foil was employed as the counter electrode (2.5 × 2.5 cm^2), meanwhile the saturated Ag/AgCl served as the reference electrode. A Na_2SO_4 solution of 0.25 M was chosen as the supporting electrolyte. Linear sweep voltammetry (LSV) was performed at a sweep rate of 100 mV s^{-1} over the potential range from 0 V to 3 V. Electrochemical impedance spectroscopy (EIS) measurements were performed at a potential of 2.2 V (vs. SCE) over the frequency range from 10^4 Hz to 10^{-2} Hz with a signal amplitude of 5 mV. The EIS results were fitted using the Zview program.

The accelerated service life tests were performed by anodic polarization of the prepared electrodes at 100mA·cm^{-2} in 1M H_2SO_4 electrolyte solution at room temperature. And the accelerated life of the electrode was defined as the duration from the beginning of the test to the time at which the cell potential increased by 10 V[4].

3. RESULTS AND DISCUSSION

3.1 Morphology and structure analysis

In order to study the influence of doping concentration, the Ti/Ni-Sb-SnO_2 electrodes with different Ni concentration were investigated in detail. Fig. 1 shows the SEM images of the freshly prepared Ti/Sb-SnO_2 electrode and Ti/Ni-Sb-SnO_2 electrode 5 at% Ni doped. From the Fig.1, we can see that the surface of Ti/Sb-SnO_2 electrode exhibited the cracked-mud morphology. This typical surface morphology is attributed to the mechanical tension caused by the successive cooling processes of the anode from 823K to room temperature and the difference in the thermal expansion coefficient between the Ti substrate and the coatings[4,34-40]. This allows the oxygen atoms to easily penetrate into the titanium surface. And the penetration of oxygen atoms can form nonconductive TiO_2 layer during the process of electrolysis. TiO_2 layer would change of interfacial tension of Ti substrate and result in peeling of the coating. In contrast with Fig.1 (a), cracks reduced dramatically in the Ti/Ni-Sb-SnO_2 electrode as shown in Fig. 1(b). This could indicate that the porous structure of Ti surface created during the pre-treatment are mainly covered. The smooth surface with fewer cracks might prevent the penetrating of electrolyte and generating bubbles to protect Ti substrate from the exposed oxidization, thus it was conducive to further improve the stability of the electrodes. This is in direct relation to the stability of the anode since the service life of these anodes is increased and will be discussed later.

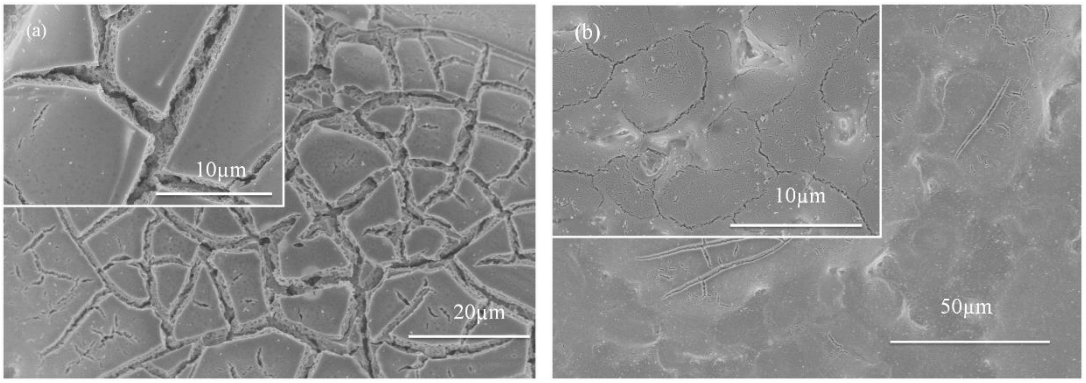

Figure 1. SEM images of (a) Ti/Sb-SnO_2 electrode and (b) Ti/Ni-Sb-SnO_2 electrode doped with 5 at.% nickel

The XRD patterns of different Ni-Sb co-doping concentration are shown in Fig.2. The peaks corresponding to (110), (101), (200), (211) and (221) diffraction of SnO_2 are observed, which is in agreement with the standard JCPDS data (File no. 41-1445). This indicates that coatings have polycrystalline nature with SnO_2 rutile structure. Furthermore no Sb-related or Ni-related oxides on these electrodes are detected, suggesting that Sb/Ni was incorporated into the SnO_2 lattice, because Sn^{4+} ions, and Ni^{2+} ions have similar ionic radius (Sn^{4+} is 0.71 Å and Ni^{2+} is 0.69 Å), so Ni^{2+} is more likely to get into the SnO_2 crystal and replace Sn^{4+}. Moreover, all samples contain sharp peaks corresponding to the hexagonal Ti substrate and no TiO_2 peaks were detected, indicating that the coating has covered Ti substrates better. By comparing the diffraction intensity, we can clearly see that as the Ni doping concentration increasing, all the peaks intensity receded gradually. It indicated that Ni^{2+} could induce

defects and distortion in the SnO_2 crystal. So the crystalline structure deteriorated when we introduced Ni.

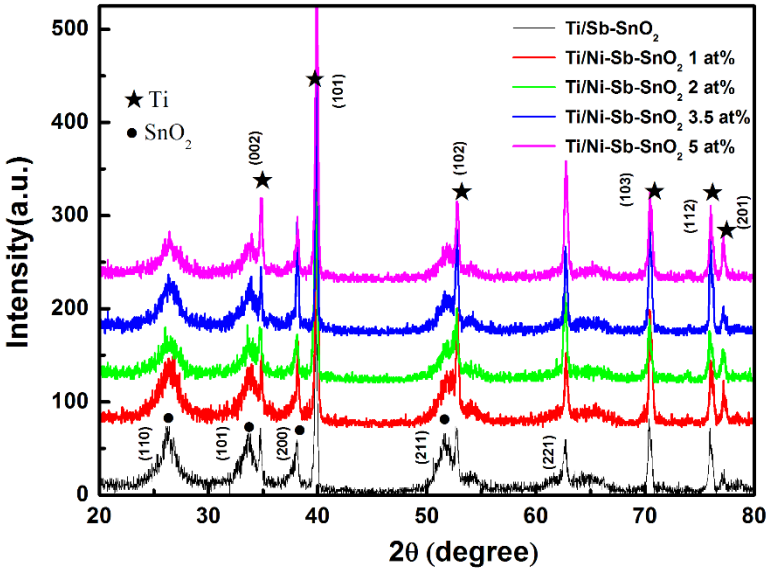

Figure 2. XRD patterns of Ti/Sb-SnO_2 electrode and Ti/Ni-Sb-SnO_2 electrodes with different nickel doping concentrations.

The particle sizes of electrode coatings were calculated using Scherer equation(35):

$$D = \frac{0.9\lambda}{\beta \cos\theta} \quad (1)$$

In eq (1), λ is X-ray wavelength; θ is diffraction angle; β is full width at half maximum (FWHM), respectively. The average crystallite sizes decreased with different Ni doping concentration, which were about 44.51, 41.85, 30.04, 24.30 and 25.63 nm, respectively. The smaller crystallite size could be favorable to improve electrochemical activity of the electrodes.

3.2. XPS analysis

XPS was conducted to verify the existence of dopants on the surface of electrodes (i.e. Sb and Ni), illuminate their chemical valence as shown in Fig.3. The binding energy (BE) for all samples was corrected by the standard C 1 s peak at 285.0 eV. From the overall survey patterns (Fig. 3(a)), we can see that all samples contain Sn, Sb, Ni, O, C, and no residue chlorine was detected, indicating that all the doping species existed in oxide forms. The BE of Sn 3d5/2 and Sn 3d3/2 at Ti/Sb–SnO_2 anode is 487.20 and 495.71eV respectively, meaning that the valence state of Sn was mainly +4 in the form of SnO_2. Because Ni is the acceptor impurity, the BE of Sn shifted to a lower energy after Ni doping, suggesting an increase of the valence charge around Sn and a decrease of the BE of inner orbital electrons[23, 24]. From Fig. 3(c), Ni 2p locates at 855.7 eV, indicating that Ni existed as +2 in the form of NiO or $Ni(OH)_2$. Because of the overlapping of O1s and Sb 3d5/2, we generally use the Sb 3d3/2 line

to determine the valence of Sb. The BE of Sb 3d3/2 is at about 540.6 eV on both electrodes, indicating that the valence of Sb was +5 in the form of Sb_2O_5 (Fig. 3d). The mixed spectra of Sb 3d5/2 and O 1s (from 528.0 to 534.0 eV) were fitted into three peaks using XPS peak (Fig. 3e–f).

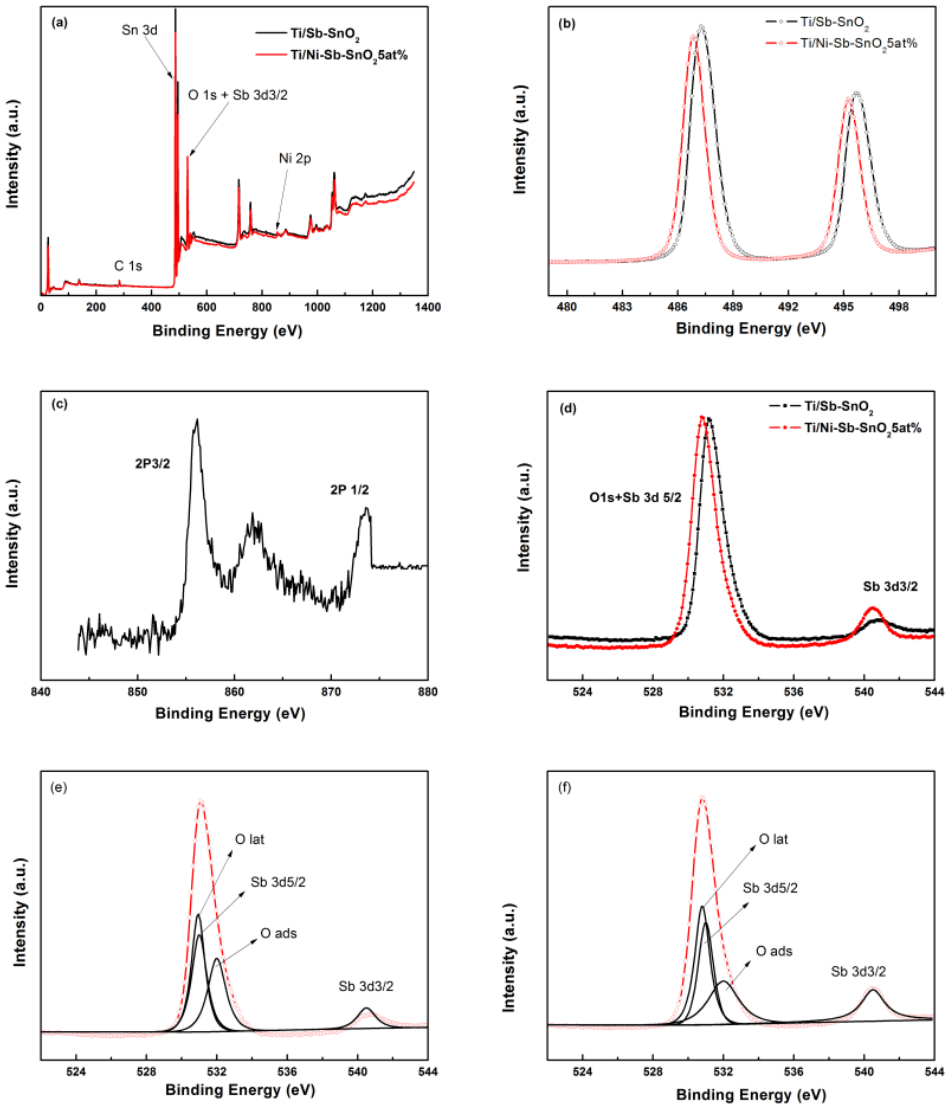

Figure 3. XPS spectra: (a) survey scanning; (b) Sn 3d; (c) Ni 2p spectra for the Ti/Ni-Sb-SnO_2 electrode with 5at%; (d) Sb 3d and O 1 s (e) fitted curves of O1s and Sb3d XPS spectra of Ti/Sb–SnO_2 electrode; (f) fitted curves of O1s and Sb3d XPS spectra of Ti/Ni-Sb–SnO_2 electrode

After deconvolution, two O 1 s bands located around 530.78 and 532.11 eV were found. The relative lower BE value (530.78 eV) of O 1 s is attributed to the lattice oxygen (O_{lat}) which are incorporated into SnO_2 crystal lattice; whereas the higher BE peak (532.11 eV) is originated from the adsorbed oxygen (O_{ads}) which is adsorptive O_2 or weakly bonded oxygen species [35]. The O_{ads} is more likely be related to the redox reaction and plays a key role in electrochemical oxidation[3]. After Ni doping, the area for the O_{ads} band increased, which may enhance the electrocatalytic activity of anodes.

3.3 Electrochemical properties

The oxygen evolution potential (OEP) is an important parameter to assess the electro-catalytic ability of electrochemical oxidation. In order to investigate the impact of Ni-Sb co-doping systematically, LSV curves were investigated to examine the OEP of the electrodes. The OEP could be obtained from the intersection of the tangent and the horizontal axis. Fig. 4 displays the LSV curves of Ti/Sb-SnO_2 and Ti/Ni-Sb-SnO_2 electrodes. From the LSVcurves, we can clearly see the OEP increased after Ni doped. As SEM observed, the crack of electrodes decreases after Ni doping, which could provide higher surface areas with more active reaction sites. This indicates that the electro-catalytic activity of the electrode increases and the corresponding oxygen evolution potential increases [37]. Then, previous reports showed that the anodes with higher OEP always have low electrode-hydroxyl radical interactions, and vice versa[20,41-43]. Hydroxyl radicals which absorbed on the electrode surface may cause the oxygen evolution, including the following reactions:

$$H_2O + MO_x \xrightarrow{surface} MOx\left(^{\bullet}OH\right)_{ads} + H^+ + e^- \quad (1)$$

$$MO_x\left(^{\bullet}OH\right)_{ads} \rightarrow 1/2O_2 + MO_x + H^+ + e^- \quad (2)$$

These active radicals also can react with organic pollutants(R):

$$MO_x\left(^{\bullet}OH_{ads}\right) + R \rightarrow MO_x + CO_2 + H_2O + \ldots. \quad (3)$$

From the above formula, we can see that the reaction (2) and reaction (3) are two competing reactions. When OEP is large enough, the reaction (2) is inhibited, and instead reaction (3) will occur easily.

The value of OEP depends on the strength of interaction between electrodes and hydroxyl radicals. As we all know, intrinsic SnO_2 is an n-type semiconductor due to V_O defect[41]. In the case of Sb-doped, Sb acts donor and forms the donor energy level. Thus the Fermi level (E_F) moves to the bottom of conduction band edge (E_C). When semiconductor contacted with metal, the band bends and a built-in field (V_b) is produced, as shown schematically in Fig. 5. The V_b can be expressed as:

$$V_b = W_s - W_m \quad (4)$$

$$W_S = E_0 - (E_F)s \quad (5)$$

$$W_m = E_0 - (E_F)m \quad (6)$$

Where W_m is the metal work function, W_s is the semiconductor work function, E_0 represents the energy of a stationary electron in a vacuum, $(E_F)_m$ and $(E_F)_s$ are Fermi levels for metals and semiconductors, respectively. The work function value for Ti and Ni are 3.85 and 4.5 eV, respectively. The work function value for intrinsic SnO_2 (4.7-5.7 eV) which is larger than that corresponding to metal contacts of Ti as 3.85 eV. Therefore, the oxygen evolution potential (V) can be written as:

$$V = V_b + V_e \quad (7)$$

where V_e is the discharge water. In the case of Sb-doped, the Fermi energy shifts into the conduction band, resulting in a lower work function of about 4.3 eV. Because doped Ni atoms generate holes, this leads to an increase in the hole concentration, compensating the electron concentration and reducing the film conductivity [44]. Hence, from the Eq. (4)-(7), we can include that the work function value for the co-doped films increased. The weak electrode-hydroxyl radical interaction on the surface of electrodes leads to a high OEP [20,28,42,43]. So we could deduce that the higher OEP results from the dense surface and the built-in potential of the mental-semiconductor contact.

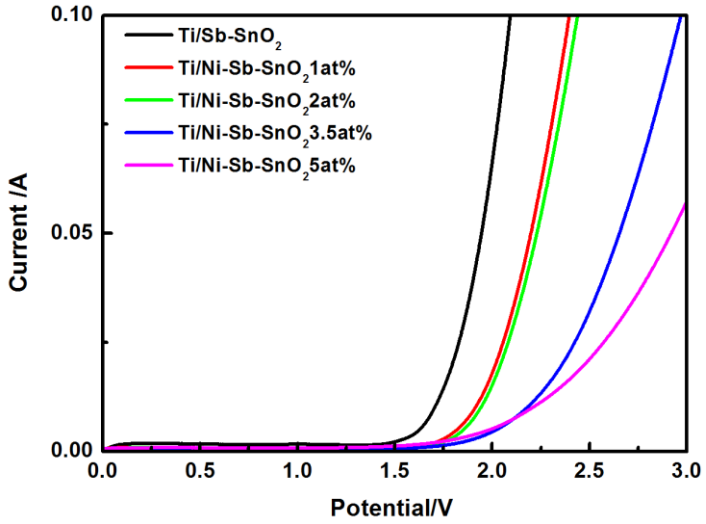

Figure 4. Linear sweep voltammetry curves of Ti/Ni-Sb-SnO_2 electrodes with different nickel doping concentrations.

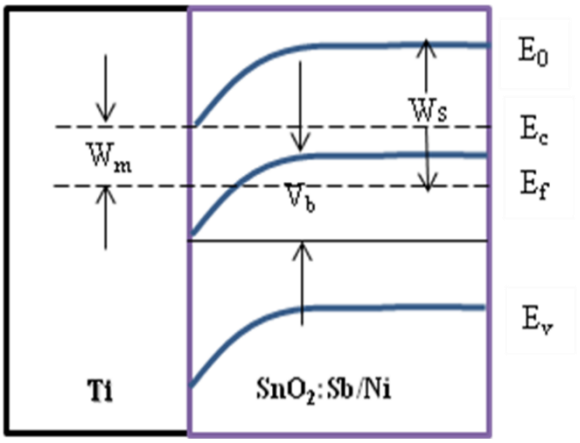

Figure 5. Schematic diagram for the band structure of the metal-semiconductor contact.

EIS is the most effective method to study the interfacial properties of the doped electrodes. As shown in Fig. 6, the Nyquist plots of the five electrodes, which were recorded between 100 kHz and 0.01Hz at a potential 2.2 V(vs.SCE), have similar shapes, indicating that they have similar surface area and morphology. Generally, electrodes with large surface area tend to have better electrocatalytic activity. The equivalent circuit model, R_s (R_{ct}CPE), which is often used to depict the electrochemical behaviors of electrodes by Zview software, was employed for fitting the EIS spectra as shown in Fig.6b. In this circuit, Rs and Rct represent the invariable solution resistance at high frequency and the charge transfer resistance during the oxygen evolution process respectively; the CPE is defined by CPE-T and CPE-P according to the formula[45]:

$$Z = \frac{1}{T(i\omega)^p} \tag{6}$$

where T is a frequency independent term with units of (mF/cm^2), ω is the angular velocity and i is the imaginary component ($i = (-1)^{1/2}$). The value of the P exponent ranges between 0 and 1. The values of CPE-P are all close to 0.9 indicating that the CPE component is close to a pure capacitor for all five electrodes. The parallel combination of the charge-transfer resistance (R_{ct}) and the constant phase element (CPE) takes into account the oxygen evolution on the electrode coatings. And it leads to a depressed semicircle in the corresponding Nyquist impedance plot. This semicircle can be ascribed to the process of charge exchange and compensation at the coating/electrolyte interface and the depressed semicircle arc in the corresponding Nyquist impedance plot represents the charge-transfer resistance R_{ct} [17,19,32-36]. The fitting results are shown in Table 1. And all the associated errors are within 8%, suggesting that the simulative circuit can fit the experimental data very effectively.

Seeing from the Nyquist plots, it can be obviously seen that the diameter of the semi-circle of Ti/Ni-Sb-SnO_2 electrode with 5 at% Ni doped (54.67Ω) is much bigger than Ti/Sn-SnO_2 (1.139Ω) electrode, indicating that the charge-transfer resistance increased through Ni/Sb co-doped. After Ni-Sb co-doped, the Rct increased dramatically, which increases the resistance of oxygen evolution. All these are consistent with polarization curve test results. These results further demonstrated that the Ti/Ni-Sb-SnO_2 electrodes have better electrocatalytic activity.

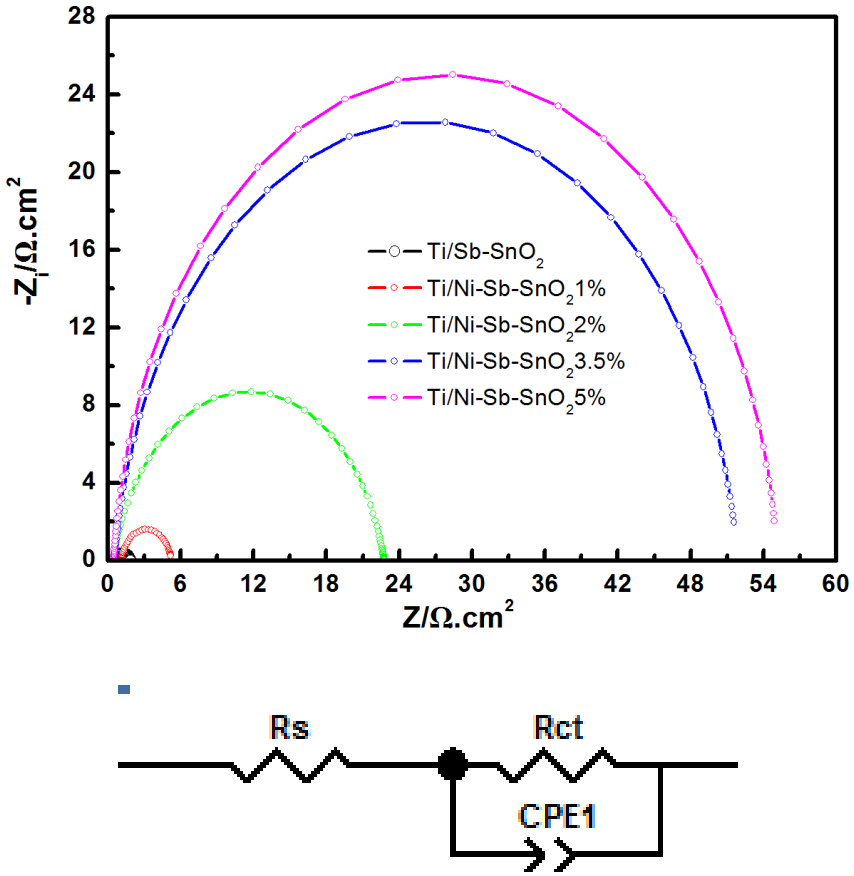

Figure 6. (a) EIS plots measured at the electrode potential 2.2 V vs SCE of the Ti/Ni-Sb-SnO_2 electrodes with different nickel doping concentrations in 0.5 M Na_2SO_4 before the lifetime test; (b) Equivalent circuit used in the simulation.

Table 1. EIS fitting analysis results of each electrode

Electrode	R_s (Ω)	R_{ct} (Ω)	CPE-T(F)	CPE-P (F)	Error (%)
Ti/Sb-SnO_2	0.73247	1.139	1.012444	0.7393	1.9166
Ti/Ni-Sb-SnO_2 (1at%)	1.096	4.184	0.00047399	0.8274	0.49879
Ti/Ni-Sb-SnO_2 (2at%)	1.197	22.35	0.00071498	0.84277	0.03021
Ti/Ni-Sb-SnO_2(3.5at%)	1.043	51.33	0.00013988	0.91978	0.14423
Ti/Ni-Sb-SnO_2 (5at%)	1.114	54.67	0.00012106	0.93835	0.05708

In view of the practical application of electrodes, electrochemical stability is a very important factor. We investigated the stability of electrodes through accelerated service life experiments. The anode potential is recorded as a function of time, and it indicates that the electrode is deactivated when the potential increases steeply[46-47], as shown in Fig.7. It can be clearly observed that the service lifetime of Ti/Ni-Sb-SnO_2 with 5 at% doped is almost 8 h, which is about 2.67 times longer than that of Ti/ Sb-SnO_2. The improved service lifetime could be attributed to the introduction of Ni. On the one hand, the coating surface is compact with small crystalline grain size which is proved in Fig. 1; on the other hand, the introduction of Ni improves the conductivity of electrodes, which could lower the potential of electrodes, and thereby reduce the generation rate of the active species. The factors that affect the stability of the Ti/Sb-SnO_2 have been studied repeatedly. Some researches demonstrated that the deactivation mechanism of Ti/Sb–SnO_2 electrode is the formation of an insulating TiO_2 layer due to the oxidation of the Ti substrate[19]. Another possible reason is the coating consumption, such as chemical consumption, electrochemical consumption and erosion. In the thermal decomposition process, the formation of random TiO_2 results in uneven interface between Ti substrate and SnO_2–Sb_2O_5 coatings. This causes coating consumption due to the different surface tension on the active sites[27]. So we discussed the electrode deactivation process in the following section.

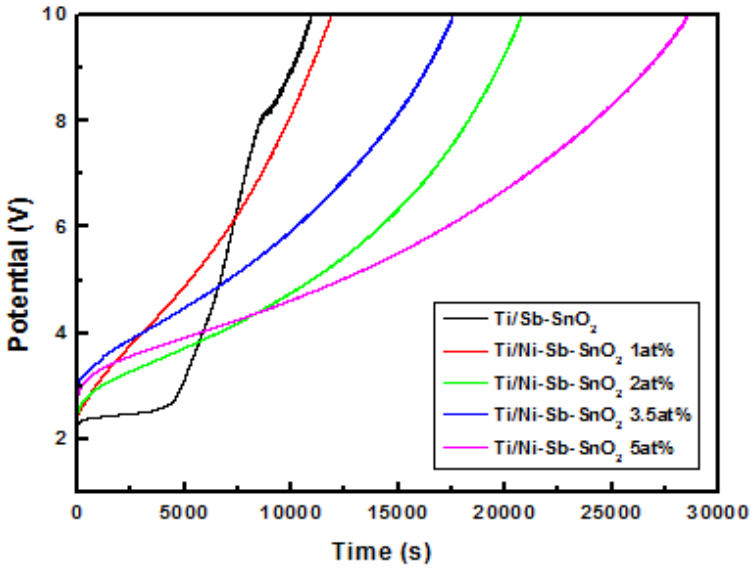

Figure 7. Accelerated service life curves of Ti/Sb-SnO_2 electrodes and Ti/Ni-Sb-SnO_2 electrodes with different nickel doping concentrations.

3.4 Failure Mechanisms of the Electrodes

In this paper, to understand the failure mechanism, we further investigated the electrodes by combining the SEM and EIS studies. Firstly, we investigated the EIS of fresh and deactivated electrodes. The corresponding fitting curves are shown in Figures 8. As shown in Fig.8, we can clearly see a big increase in the diameter after the electrode is deactivated, and the R_{ct} of the deactivated one (136Ω) was almost 16 times more than the fresh one (8.602Ω). To further understand these changes, we investigated morphology of the deactivated electrodes using SEM. Fig. 9b shows the SEM images of the electrodes after the accelerated service life tests. In comparison with the fresh electrode (as shown in Fig. 9a, it could be seen that the surface of the electrodes has been destroyed and there were many cracks and holes on the coatings, moreover some of the coatings have fallen apart. And the cracks extended through the coating, which can be related to erosion provoked by the oxygen evolution reaction during the anodic polarization of the electrode, resulting in detachment of the coating from the electrode surface. But from the SEM micrographs, we could find that there was still a considerable amount of coating on the electrode surface. Furthermore, we did XPS to verify this point, as shown in Fig. 10. The element composition of the electrode is not very obvious. All these indicated that the deactivation of electrodes maybe mainly originated from passive TiO_2 interlayer and coating consumption. The passive TiO_2 interlayer formed on the Ti surface which may blocks the charge transfer leading to the increase of potential and result in the deactivation of electrodes [19-20].

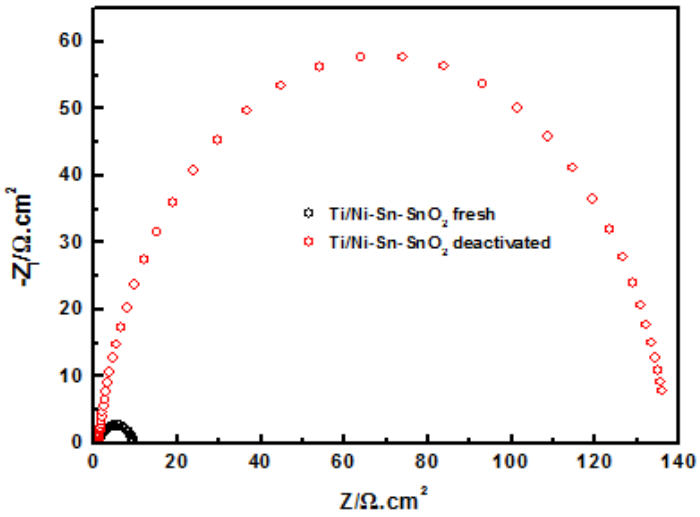

Figure 8. EIS complex plane plots: (a) freshly prepared electrode; (b) the deactivated electrode.

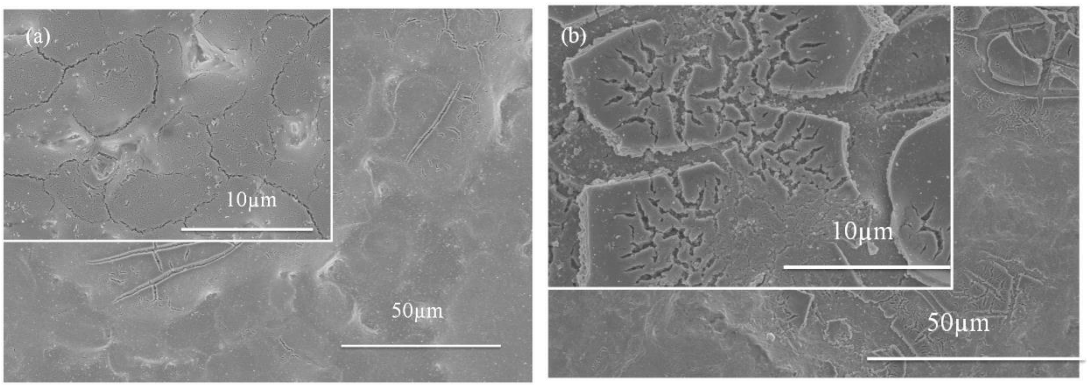

Figure 9. SEM images: (a) freshly prepared electrode; (b) the deactivated electrode.

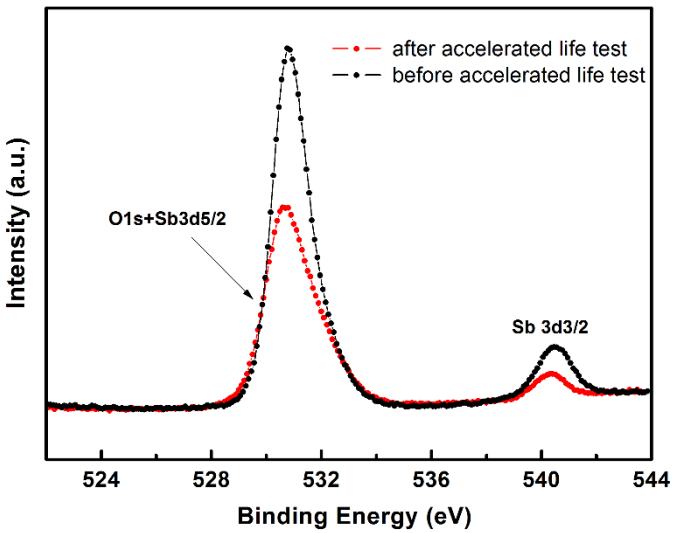

Figure 10. XPS spectra: Sb 3d and O 1 s spectra on the surface of Ti/Ni-Sb-SnO_2 electrode before accelerated and after accelerated life test.

4. CONCLUSION

We prepared the Ti/Ni-Sb-SnO_2 electrodes by coating pyrolysis method. The morphologies, microstructures and the surface elements' chemical states of Ti/Ni-Sb-SnO_2 electrodes were investigated through SEM, XRD and XPS. We also studied the electrochemical properties of Ti/Ni-Sb-SnO_2 electrodes using LSV and EIS tests. Moreover, we investigated the failure mechanism of the Ti/Ni-Sb-SnO_2 electrodes. The main conclusions of this work can be summarized in the following points:

• The Ti/Ni-Sb-SnO_2 electrodes have a more compact surface with fewer cracks;

• The oxygen evolution potentials of Ti/Ni-Sb-SnO_2 electrodes improved from 1.830 to 2.342 eV;

• The deactivation of Ti/Ni-Sb-SnO_2 electrode was mainly due to the formation of a passive TiO_2 interlayer between the Ti substrate and the coating.

ACKNOWLEDGEMENTS
This work is supported by the fund of Beijing Key Discipline of Condensed Matter Physics (Grant no. 0114023).

References

1. S. Y. Yang, Y. S. Choo, S. Kim, S. K. Lim and J. Lee, H. Park, *Appl. Catal., B,* 111-112 (2012) 317.
2. S. Ferro, D. Rosestolato, C. A. Martínez-Huitle and A. De Battisti, *Electrochim. Acta,* 146 (2014) 257.
3. Y.-H. Cui, Y.-J. Feng and Z.-Q. Liu, *Electrochim. Acta,* 54 (2009) 4903.
4. C. Shao, A. Chen, B. Yan, Q. Shao and K. Zhu, *J. Electroanal. Chem.,* 778 (2016) 7.
5. X. Chen and G. Chen, *Electrochim. Acta,* 50 (2005) 4155.
6. J. P. F. Matos, L. Proença, M. I. S. Lopes and I. T. E. Fonseca, *J. Electroanal. Chem.,* 571 (2004) 111.
7. J.-M. Hu, J.-Q. Zhang, H.-M. Meng, J.-T. Zhang and C.-N. Cao, *Electrochim. Acta,* 50 (2005) 5370.
8. S. Kim, S. K. Choi, B. Y. Yoon, S. K. Lim and H. Park, *Appl. Catal., B,* 97 (2010) 135.
9. F. F. Marco Musiani and Renzo Bertoncello, *J. Electroanal. Chem.,* 465 (1999) 160.
10. T. T. Hideo Notsu and Akira Fujishima, *J. Electroanal. Chem.,* 523 (2002) 86.
11. P. A. M. M. Panizza, G. Cerisola and C. Comninellis, *Electrochem. Commun.,* 3 (2001) 336.
12. Y. Tian, X. Chen, C. Shang and G. Chen, *J. Electrochem. Soc.,* 153 (2006) J80.
13. X. Y. Li, Y. H. Cui, Y. J. Feng, Z. M. Xie and J. D. Gu, *Water Res.,* 39 (2005) 1972.
14. C. P. Ch. *Comninellis, J. Appl. Electrochem.,* 23 (1993) 108.
15. X. Chen, F. Gao and G. Chen, *J. Appl. Electrochem.,* 35 (2005) 185.
16. H.-y. Ding, Y.-j. Feng and J.-f. Liu, *Mater. Lett.,* 61 (2007) 4920.
17. L. Xu, M. Li and W. Xu, *Electrochim. Acta,* 166 (2015) 64.
18. X. Cui, G. Zhao, Y. Lei, H. Li, P. Li and M. Liu, *Mater. Chem. Phys.,* 113 (2009) 314.
19. Aicheng Chen and Stephanie Nigro, *J. Phys. Chem. B,* 107 (2003) 13341.
20. Cairu Shao, Jiangang Yu, Xia Li, Xiyuan Wang and Kaigui Zhu, *J. Electroanal. Chem.,* 804 (2017) 140.
21. A. I. del Río, J. Fernández, J. Molina, J. Bonastre and F. Cases, *Electrochim. Acta,* 55 (2010) 7282.
22. Y. H. Wang, K. Y. Chan, X. Y. Li and S. K. So, *Chemosphere,* 65 (2006) 1087.
23. Z. Sun, H. Zhang, X. Wei, X. Ma and X. Hu, *J. Solid State Electrochem.,* 19 (2015) 2445.
24. Z. Sun, H. Zhang, X. Wei, R. Du and X. Hu, *J. Electrochem. Soc.,* 162 (2015) H590.

25. F. Montilla, E. Morallón and J. L. Vázquez, *J. Electrochem. Soc.,* 152 (2005) B421.
26. Guohua Chen, Xueming Chen and Po Lock Yue, *J. Phys. Chem. B,* 106 (2002) 4363.
27. D. He and S.-i. Mho, *J. Electroanal. Chem.,* 568 (2004) 19.
28. H. Shekarchizade and M. K. Amini, *Int. J. Electrochem.,* 2011(2011).
29. Aqing Chen, Xudong Zhu, Junhua Xi, Haiying Qin, Zhenguo Ji and Kaigui Zhu, *J. Alloys Compd.,* 684 (2016) 137.
30. Y.-H. Wang, S. Cheng, K.-Y. Chan and X. Y. Li, *J. Electrochem. Soc.,* 152 (2005) D197.
31. Paul Andrew Christensen, Khalid Zakaria, Henriette Christensen and Taner Yonar, *J. Electrochem. Soc.,* 160(8) (2013) H405.
32. P.A. Christensen and A. Imkum, *Ozone: Sci. Eng.,* 33 (2011) 389.
33. P.A. Christensen, W.F. Lin, H. Christensen, A. Imkum, J.M. Jin, G. Li and C.M. Dyson, *Ozone: Sci. Eng.,* 31 (2009) 287.
34. J.-t. Kong, S.-y. Shi, X.-p. Zhu and J.-r. Ni, *J. Environ. Sci.,* 19 (2007) 1380.
35. T. Duan, Q. Wen, Y. Chen, Y. Zhou and Y. Duan, *J. Hazard. Mater.,* 280 (2014) 304.
36. T. Pajkossy, *J. Electroanal. Chem.,* 364 (1994) 11.
37. Y. Duan, Y. Chen, Q. Wen and T. Duan, *J. Electroanal. Chem.,* 768 (2016) 81.
38. J. Fan, G. Zhao, H. Zhao, S. Chai and T. Cao, *Electrochim. Acta,* 94 (2013) 21.
39. L.M. Da Silva, L.A. De Faria and J.F.C. Boodts, *J. Electroanal. Chem.,* 532 (2002) 141.
40. H. Xu, A.-P. Li, Q. Qi, W. Jiang and Y.-M. Sun, *Korean J. Chem. Eng.,* 29 (2012) 1178.
41. K. Galatsis, L. Cukrov, W. Wlodarski, P. McCormick, K. Kalantar-zadeh, E. Comini and G. Sberveglieri, *Sens. Actuators, B,* 93 (2003) 562.
42. Aqing Chen, Bin Bin Li, Bojan Miljkovic, Christina Souza, Kaigui Zhu and Harry E. Ruda, *Appl. Phys. Lett.,* 105 (2014) 021606.
43. Christos. Comninellis and Guohua. Chen, Electrochemistry for the Environment, Springer-Verlag New YorkInc, (2010) Springer New York Dordrecht Heidelberg London, England.
44. Xia Li, Rui Deng, Yongfeng Li, Bin Yao, Zhanhui Ding, Jieming Qin and Qingcheng Liang, *Ceram. Int.,* 42 (2016) 5299.
45. Brian Adams, Min Tian and Aicheng Chen, *Electrochim. Acta,* 54 (2009) 1491.
46. F. Montilla, E. MorallÓn, A. De Battisti and J. L. Vázquez, *J. Phys. Chem. B,* 108 (2004) 5036.
47. Lichao Zhang, Li Xu, Jing He and Jiejing Zhang, *Electrochim. Acta,* 117 (2014) 192.